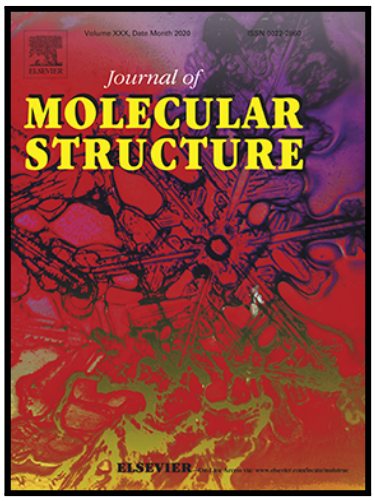

Lead Ion Selective Electrodes from Dibenzo-18-crown-6 derivatives: An exploratory study

Deneikah T. Jackson , Peter N. Nelson , Irvin N. Booysen

PII: S0022-2860(20)31889-5
DOI: https://doi.org/10.1016/j.molstruc.2020.129575
Reference: MOLSTR 129575

To appear in: *Journal of Molecular Structure*

Received date: 7 September 2020
Revised date: 31 October 2020
Accepted date: 2 November 2020

Please cite this article as: Deneikah T. Jackson , Peter N. Nelson , Irvin N. Booysen , Lead Ion Selective Electrodes from Dibenzo-18-crown-6 derivatives: An exploratory study, *Journal of Molecular Structure* (2020), doi: https://doi.org/10.1016/j.molstruc.2020.129575

Highlights

- Dibenzo-18-crown-6 and its derivatives spontaneously coordinate with lead(II) ions.
- All derivatives form stable electropolymerized films or chemisorbed monolayers on the electrode surface.
- Aromatic ring chemistry influences the lead(II) sensing behaviour of all electrodes.
- All modified electrodes allow quantification of lead(II) ions below 10 ppm.

Lead Ion Selective Electrodes from Dibenzo-18-crown-6 derivatives: An exploratory study

[a]Deneikah T. Jackson, [a]Peter N. Nelson*, [b]Irvin N. Booysen

[a]University of the West Indies Mona, Department of Chemistry, Faculty of Science and Technology, Kingston 7, St. Andrew, Jamaica.

[b]School of Chemistry and Physics, University of KwaZulu-Natal, Private Bag X01, Scottsville, Pietermaritzburg, 3209, South Africa.

Abstract

Dibenzo-18-crown-6 (DB18C6) and three of its derivatives (-$COCH_3$, -Br, -NO_2), are investigated *via* Density Functional Theoretical (DFT) modelling, Fourier Transform Infrared (FT-IR) and absorption spectroscopies, Differential Pulse Anodic Stripping (DPASV), Cyclic (CV) and Square Wave (SWV) voltammetries, as possible materials for preparing plasticiser free lead(II) ion selective electrodes. The spontaneous, entropy driven, interactions between lead(II) ions and DB18C6 derivatives are such that they form 1:1 complexes *via* coordination with the high electron density open ether cavity, except for the brominated derivative where the metal: ligand stoichiometry is 2:1 due to exo-cavity coordination *via* the high electron density bromine atoms. Monolayers resulting from electropolymerization of some derivatives (-H, -$COCH_3$, -Br) and chemisorption of the -NO_2 derivative, allows quantification of lead(II) ions at concentrations below 10 mg L^{-1} with minimal interference from other metal ions except Hg^{2+} and Al^{3+}.

Keywords: Lead(II); Electropolymerization, Dibenzo-crown; Density-Functional-Theory.

Send correspondences to Peter Nelson

e-mail: peter.nelson02@uwimona.edu.jm

Tel: (876) 927 - 1910

1 Introduction

Metal ions are environmentally ubiquitous, arising from numerous natural as well as synthetic/ man-made processes. For instance, increased industrialization, coupled with the continuous advancement in technology, over the last three decades, have encouraged an astronomical increase in manning activities, leading to increase exposure of ground water, flora and fauna to toxic heavy metals such as lead, arsenic, cadmium, mercury, chromium, copper, chromium and others [1,2,3,4]. The toxicity of such species highlights the need for highly sensitive methodologies, offering cheap and convenient detection of same. Hence, complexiметric techniques, applying various ligand systems, have been investigated by numerous researchers for the colorimetric and electrochemical detection of various heavy metals [5,6,7,8]. Host-guest complexes of macrocyclic organic molecules such as calixarenes [9,10,11,12]. Cryptands [13,14,15,16] and crown ethers [17,18,19,20,21] have been investigated as possible complexing agents for the detection, quantification and sequestration of heavy metals. However, though the reports on these systems indicate some level of success, poor selectivity and low sensitivity remains a challenge. Nonetheless, it has been demonstrated that the type of coordinating atoms can significantly affect the selectivity of these systems. For instance, it has been demonstrated that for the detection of lead(II) ion *via* complexiметry, sulphur atoms, single or double bonded, allows tremendous selectivity [22,23,24,25,25b,26]. The charge density (hardness or softness) of the analyte ion relative to the donor atom, has also been demonstrated to be a useful parameter for controlling selectivity [27].

Crown ether type systems such as dibenzo-18-crown-6 (DB18C6) represent an interesting starting point for development of high selectivity complexiметric reagents because of their ability to size bind and also to alter their molecular structure to accommodate ions that are larger than their cavity size [28,29,30,31]. However, though various studies have been carried out on crown ethers and DB18C6 in particular, modification of the electronic structure by manipulating the substituents on the phenyl rings remains unrealized. Hence, the effects of such modification on the suitability of DB18C6 for electrode surface modification and thus use as an electrochemical sensor, remains unprobed. Furthermore, though an interesting computational study on the metal binding selectivity of DB18C6 towards alkali metals was reported by Kim and co-workers [32]. Substituent effects on metal ion selectivity was not investigated. However, the results presented therein, not only indicated that the high selectivity for potassium was a result of competition between the solvent and the cavity but

also that cheap computational techniques are capable of producing reasonable data on the metal binding behaviour of these systems.

Hence, in this paper, DB18C6 and three of its derivatives will be investigated for their ability to form stable complexes with lead(II) ions, both computationally and experimentally. Furthermore, application of DB18C6 derivatives in the surface modification of electrodes for the electrochemical quantification of lead(II) ions, as presented in this paper, represent the use of an experienced method with a novel tool for the sensing of this heavy metal which has been a major cause for concern in many countries such as the United States of America [33,33b,34] and Canada [35], in recent times.

2 Experimental

2.1 Synthesis

All compounds were synthesized as depicted in scheme 1.

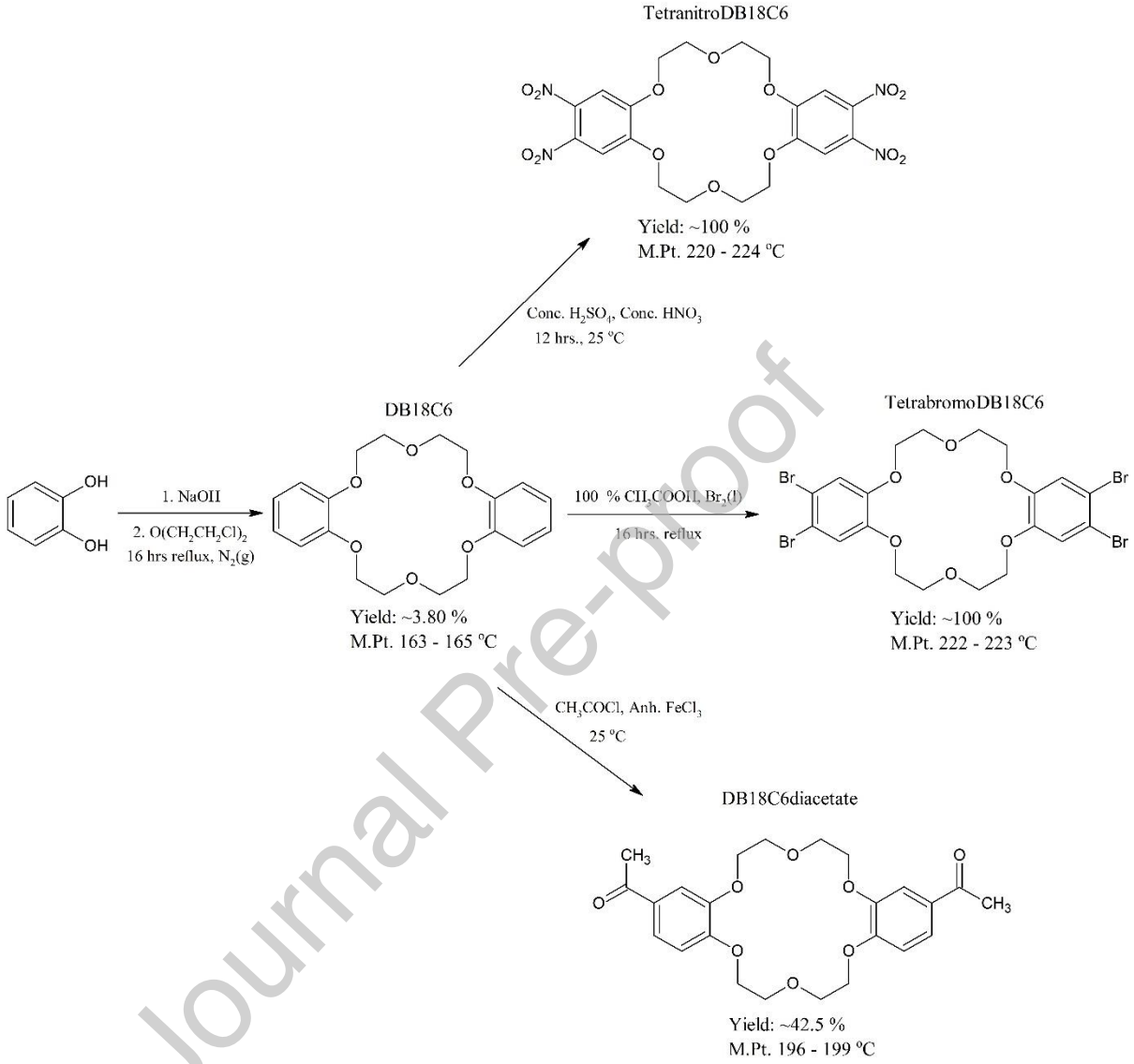

Scheme 1. Synthetic scheme for DB18C6 and three of its derivatives.

Dibenzo-18-crown-6 (DB18C6)

To an n-butanol solution of catechol (11.9926 g, 0.1089 mol), containing sodium hydroxide (4.4943 g, 0.1124 mol), an n-butanol solution of 2, 2-dichlorodiethyl ether (8.0508 g, 0.0563 mol) was added drop-wise with continuous stirring and heating over a 2 hrs. period, prior to the mixture being cooled to 90 °C and more sodium hydroxide (4.4471 g, 0.1112 mol) added. The reaction mixture was then refluxed for 16 hrs. after which the liquor was cooled then

acidified. Acetone (100 mL) was subsequently added with stirring and the resulting precipitate collected by vacuum filtration and recrystallized from acetonitrile to give an off white powder. M.Pt. 163 – 165 °C. Yield of 3.47 %. Success of the synthesis was confirmed by ^{1}H, ^{13}C NMR and FT-IR measurements (**See S1**). However, it is worthy of note that other authors [36,37], whose work was not found during the period of synthesis for this paper, were able to achieve yields of up to 48 %.

20, 25-Diethanonedibenzo-18-crown-6 (DB18C6diacetate)

Anhydrous iron (III) chloride (0.179 g, 0.0011 mol) was combined with acetyl chloride (0.8593 g, 0.0109 mol) in dichloromethane (DCM), in a 50 mL round bottom flask, to which a DCM solution of 0.2 g dibenzo-18-crown-6 (0.0005 mol) was added drop-wise over a 5 min. period. The reaction mixture was stirred at room temperature for 2 hrs., then quenched with water (5 mL) and allowed to stir for an additional 5 minutes, followed by extraction with DCM and aqueous sodium hydroxide (50 mL, 0.5 M). The solid precipitate was then collected via vacuum filtration. M.Pt. 196 - 199 °C. Yield of 42.6 %. Success of the synthesis was confirmed by ^{1}H, ^{13}C NMR and FT-IR measurements (**See S1**).

Tetranitrodibenzo-18-crown-6 (TetranitroB18C6)

Concentrated sulphuric acid (5 mL) and nitric acid (5 mL) were both added to a DCM solution of Dibenzo-18-crown-6 (0.3540 g, 0.0009 mol). The resultant mixture was stirred at room temperature for 12 hrs., following which it was neutralized with sodium hydroxide solution (8 M, ~50 mL) and the pale yellow precipitate collected via vacuum filtration. M.Pt. 220 - 224 °C. Yield 100 %. Success of the synthesis was confirmed by ^{1}H, ^{13}C NMR and FT-IR measurements (**See S1**).

20,21,24,25 Tetrabromodibenzo-18-crown-6 (TetrabromoDB18C6)

Liquid bromine (2 mL, 0.0776 mol) was added to a mixture of Dibenzo-18-crown-6, (0.8974 g, 0.0027 mol), glacial acetic acid (30 mL) and water (25 mL), in a round bottom flask, and

the resulting mixture heated to reflux for 12 hrs. The mother liquor was then cooled to ~28 ^{o}C and the resulting white precipitate collected by vacuum filtration and washed with ~20 mL of diethyl ether. Recrystallization of the precipitate was carried out in chloroform. M.Pt. 222 – 223 °C. Yield 100 %. Success of the synthesis was confirmed by ^{1}H, ^{13}C NMR and FT-IR measurements (**See S1**).

2.2 Molecular Modelling

DFT calculations, conducted using a Gaussian 16 software package [38], were carried out at the 6-311++G(d,p), 6-311++G(2d,p), 6-311G(d,p) levels of theory, where Becke's three parameter hybrid function (B3) [39] was employed for fermion exchange in addition to Lee, Yang and Parr's (LYP) correlation function: B3LYP [40], augmented for long range interactions via a Coulomb Attenuating Method: CAM-B3LYP [41]. Solution phase calculations were effected *via* the Conductor-like Polarisable Continuum Model: C-PCM [42,43], where the solute is surrounded by a dielectric of permittivity **ε**, representing the solvent. Calculations involving lead(II) were carried out *via* Las Almos National Laboratory's double zeta Effective Core Potential (ECP): LANL2DZ [44,45].

2.3 Cyclic voltammetry

All electrochemical studies were carried using a CorrTest CS350 potentiostat/ Galvanostat workstation, controlled by CS studio Software package. The applied three electrode set-up was composed of a silver-silver chloride reference whereas platinum was used for the working and counter electrodes. All measurements were carried out under a static nitrogen atmosphere.

3 Results and Discussion

3.1 Molecular Modelling and Infrared Spectroscopy

Minimum structures, calculated at the 6-311++G(d,p)/RB3LYP level of theory, indicated by the absence of imaginary frequencies in the Hessian, show that all neighbouring methylene groups of the ether chains adopt a nearly perfect *all-trans* arrangement (**Fig. 1**); the most stable configuration for such groups [46,47,48].

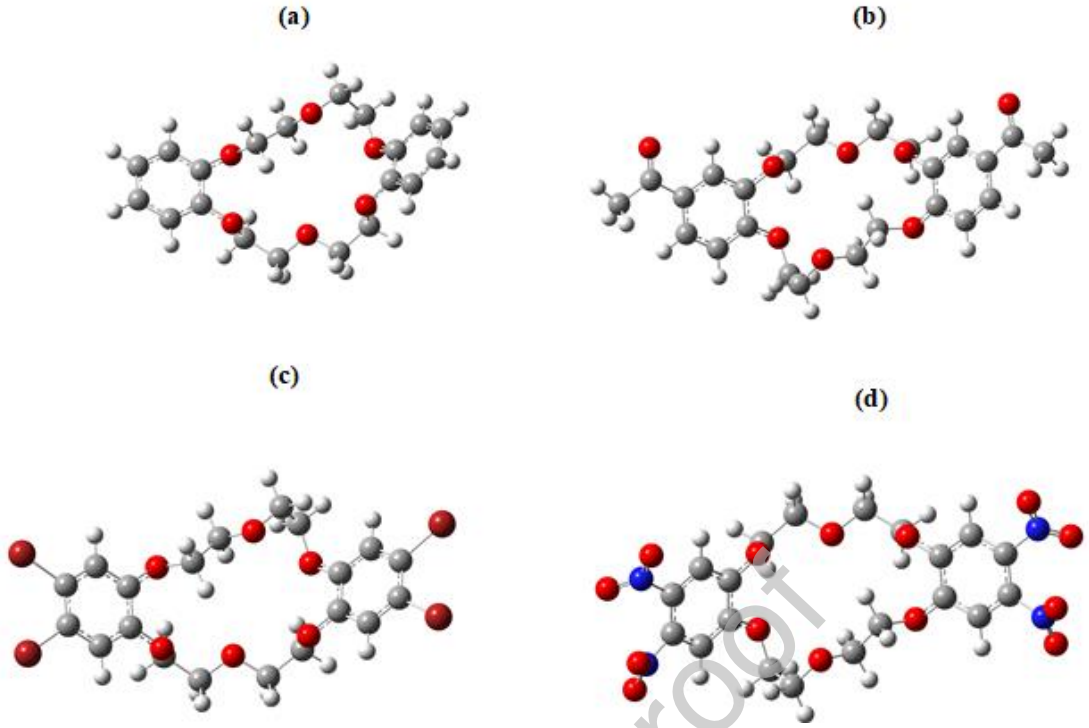

Fig. 1. Optimized structures for (a) DB18C6, (b) DB18C6diacetate, (c) tetrabromoDB18C6 and (d) tetranitroDB18C6.

However, though all CH_2 groups are arranged in this low energy configuration, the two ether chains connecting the two phenyl rings, differ considerably in their overall structure. For instance, the -OCH_2CH_2O- fragments, two of which combine to form a single ether chain, adopt different configurations (**Fig. 2**) in both chains of the ether ring; that is, for DB18C6, in one chain the dihedrals are -49.97 and -175.19 ^{o} whereas for the other chain they are 71.80 and 72.29 ^{o}; hence, these minimum structures are such that the ether cavity is open (**Fig. 1** and **Fig. 2**). Indeed, similar such angles are calculated for the other derivatives; hence, the same open cavity structure: cavities as wide as *ca*. 4.74 Å, are calculated for them. Calculated methylene C-H distances, in the range of 1.097 - 1.100 Å, are close to that expected for hydrogens attached to aliphatic carbons [49], however, the slightly shorter distances calculated here, are most likely caused by the electron withdrawing nature of the oxygen atoms. Additionally, since the calculated ether C-O distances: 1.422 Å, are typical for such systems [50], it is clear that the applied modelling chemistry is of sufficient accuracy to allow rationalization of the data presented herein. However, the C-O bond orders, where the ether chains attach to the phenyl rings, are 1.5 for all compounds; that is, these bond distances are in the range of 1.364 - 1.377 Å. This is due to conjugation between the phenyl *pi*-systems and

the *n*-electrons of the attached oxygen atoms, a clear indication that the electronic structure of the phenyl ring is influential where electron density inside the ether cavity is concerned.

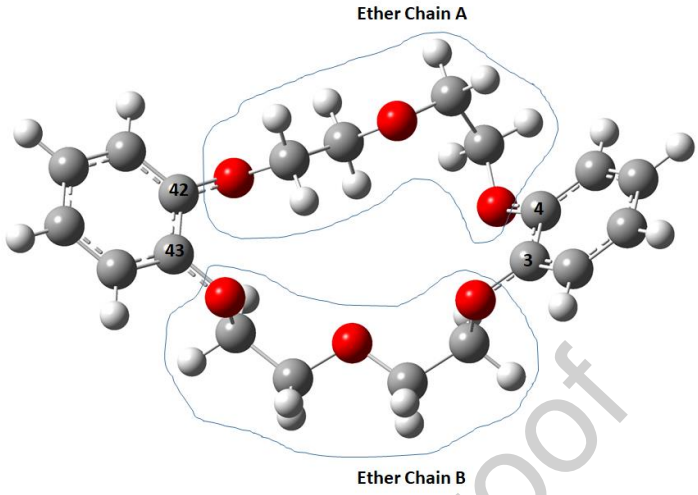

Fig. 2. Optimized structure depicting structural differences between the ether chains.

Calculated C-C distances for the phenyl rings reveal reduced symmetry. For example, in the case of DB18C6, the phenyl C-C distance between carbons to which the ether chains are attached (C42-C43 and C4 –C3, **Fig. 2**) are *ca.* 1.409 Å, whereas the other analogous C-C bond lengths are *ca.* 1.391 Å. Indeed, similar results were obtained for the other derivatives. Interestingly, all compounds show reduced symmetry due to elongation of the aromatic C-C bonds attached to the substituent baring carbons, highlighting the severity of substituent effects on the molecular structure of these compounds. Expectedly, concomitant with such variations in bond lengths, divergence between expected and calculated phenyl bond angles are observed [51]. For example, the internal angles of the phenyl rings vary from 120.49 to 119.85 ^{o}, for all compounds. However, since the force on all atoms is zero, it is clear that angle strain resulting from such variations are cancelled by variations in other regions of the rings. Surely, such peculiar structural features should be reflected in their spectroscopic properties

Hence, experimental infrared spectra were collected at ambient temperature in the solid state, for all compounds. They consist of low intensity bands in the high frequency region of 3500 - 2800 cm^{-1} and medium to high intensity bands in the low frequency region of 1700 - 500 cm^{-1} (**Fig. 3**).

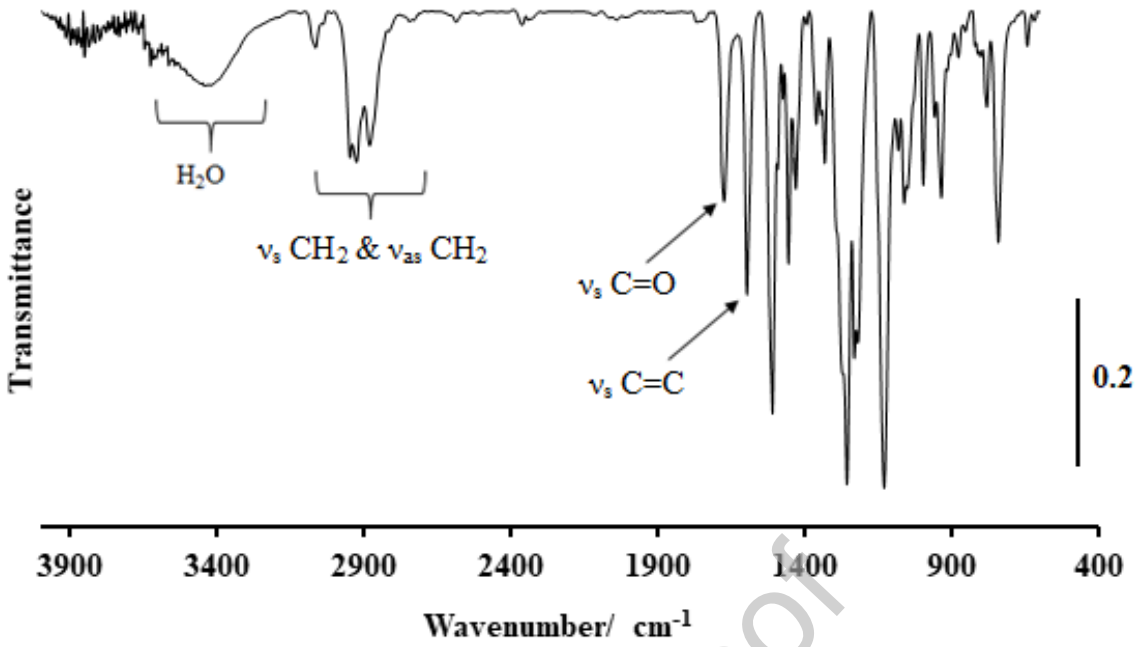

Fig. 3. Solid state FT-IR spectra for DB18C6diacetate, exhibiting features typical for dibenzo-18-crown-6 derivatives.

The broad medium intensity band, observed at ~ 3500 cm^{-1}, characteristic of the –OH stretching vibration of water molecules, is indicative of hydrated ether cavities. In fact, hydration of the ether cavity in such systems is not surprising since the oxygen atoms can facilitate hydrogen bonding, as reported elsewhere [52]. These results suggest that the samples, prepared herein, are hydrates, hence, the observed divergence between theoretical and experimentally determined elemental composition (**See S2**). Furthermore, since the relative intensities of the OH vibration is not identical for all compounds, different hydration numbers are indicated; that is, the true composition of the samples are DB18C6**.0.5**H_2O, DB18C6diacetate**.0.25**H_2O, tetrabromoDB18C6**.3**H_2O and tetranitroDB18C6**.2**H_2O. This high frequency region is also characterized by the aromatic carbon-hydrogen symmetric stretching modes ($\boldsymbol{\nu}_s$C-H), at *ca.* 3067 cm^{-1}, as expected [53], with the methylene group asymmetric ($\boldsymbol{\nu}$as) and symmetric stretching vibrations of the ether rings at *ca*. 2954 and *ca*. 2854 cm^{-1}, respectively. However, the broad and complex nature of the methylene stretching band indicates that the CH_2 groups of the ether chains are not equivalent; a proposal supported by the asymmetric nature of the minimize structures (**Fig. 1**); hence, the $\boldsymbol{\nu}_s$C-H and $\boldsymbol{\nu}_{as}$C-H modes for the ether chain segments are observed at slightly different frequencies, leading to band broadening. Calculated infrared spectra, scaled by various factors (**See S3**),

such that the experimental and calculated C=C stretching vibrations coincide, supports the hypothesis of vibrational non-equivalence among the ether CH_2 population; that is, multiple peaks are calculated in the region of 2850 to 3100 cm^{-1}, all associated with the symmetric and asymmetric C-H stretching of different regions of the ether chains, as indicated by the animated calculated spectra. Since the C=O stretching vibration for DB18C6diacetate is observed at 1674 cm^{-1} but calculated, for the isolated molecular, to be 1701 cm^{-1}, strong intermolecular interactions, in the solid state, is indicated, hence, the observed high melting point, relative to DB18C6, for this derivative. Furthermore, the asymmetric nature of both the calculated and observed ν_sC=O vibration band suggest non-equivalence of the two acetate substituents on each of the phenyl rings. Indeed, animation of the calculated spectra indicates that the peak, calculated at 1701 but observed at 1674 cm^{-1}, is composed of two energetically similar vibrations, associated with individual C=O groups. Similar effects are also observed for both the calculated and experimental ν_sC=C vibration, confirming non-equivalence of the phenyl rings; in all derivatives. For the tetranitro compound, the N=O stretching vibration is observed and calculated as a broad strong band (Full width at half maximum, FWHM, ~45 cm^{-1}). Such band broadening is due to non-degeneracy between the N=O vibrational energy levels caused by the low overall molecular symmetry. However, over estimation of the N=O vibrational energy: calculated at ca. 1608 – 1602 cm^{-1} but observed at 1535 cm^{-1}, is not only due to the harmonic nature of the calculations; partially accounted for *via* the aforementioned scaling regime, but is mostly due to the calculated N=O bond order; recognized as 1.5 but calculated as full double bonds. Interestingly, for the tetrabromo derivative, the aromatic C=C vibrations for each ring are significantly separated; that is, they are observed at 1583 and 1568 cm^{-1} but calculated at 1587 and 1581 cm^{-1}, without scaling. Overall, these results show that the calculated and experimental spectra are tremendously similar, hence, the scaling factors are in the region of 0 – 0.996; at testament of the appropriateness of the applied modelling parameters.

3.2 Uv-vis spectroscopy

Absorption spectra, collected for all compounds at ambient temperature in dimethylsulphoxide, shows up to two clear bands. For instance, the spectra for tetrabromoDB18C6 shows a single broad (FWHM = 25 nm) asymmetric absorption at 298 nm, most likely associated with a combination of the *n* to π* transitions between the aromatic rings and the bromine atoms, in addition to the π to π* transitions of the phenyl rings as

indicated by the calculated frontier molecular orbital surfaces (**Fig. 4**). However, for the tetranitro derivative, these two transitions are observed as individual bands; that is, two broad absorptions are observed at 275 and 305 nm, due to π to π* transition of the aromatic rings in addition to *n* to π* transitions between the aromatic rings and the nitro substituents, respectively.

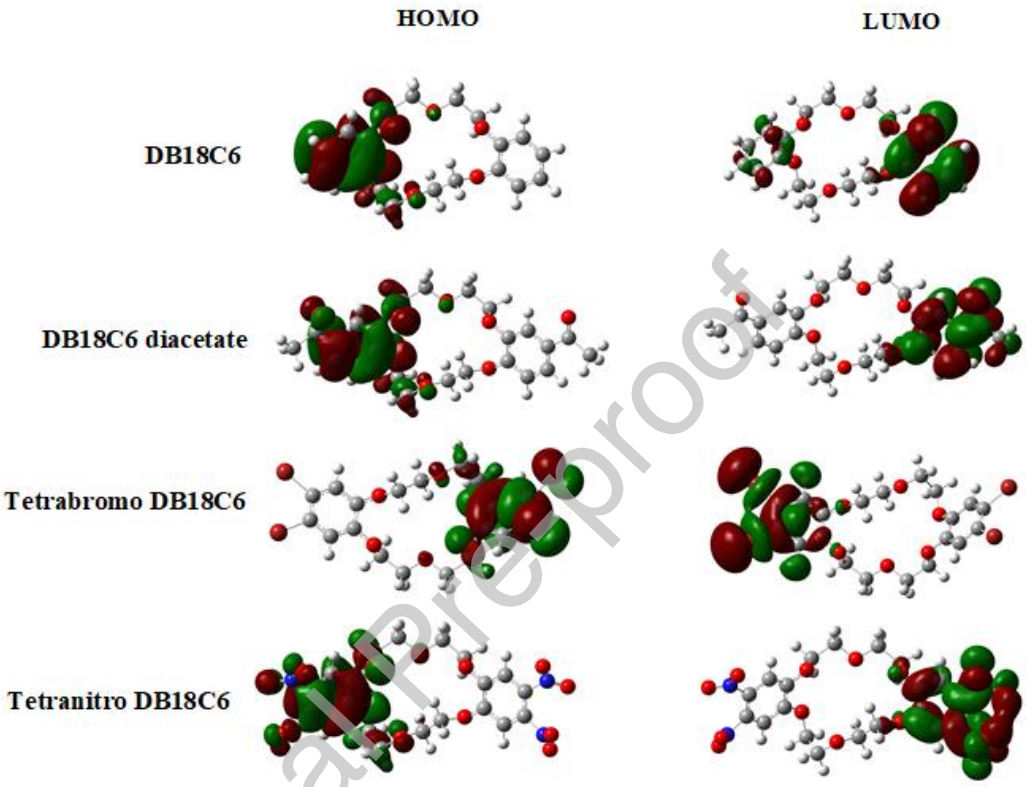

Fig. 4. Calculated frontier molecular orbital surfaces (HOMO and LUMO) for all compounds.

Similarly, for the diacetate derivative, two absorptions are obvious at 305 and 276 nm, associated with the *n* to π* transition due to electron density migration from the acetate oxygen into the conjugated aromatic - acetate π-system in addition to the higher energy π to π* transitions of the phenyl and C=O *pi*-systems, respectively. For the unmodified DB18C6, two transitions are obvious: 277 and 306 nm, emanating from the inter-aromatic ring π to π* charge transfer and the lower energy *n* to π* transitions between the ether oxygens and the aromatic π-system. Interestingly, for all compounds, the HOMO to LUMO transition is associated with charge transfer between the aromatic rings; that is, from one side of the molecule to the other (**Fig. 4**), indicating that their structural asymmetry is also reflected in their electronic structure. Indeed, electrostatic potential maps (ESPM) confirm their highly

uneven charge distribution; that is, the cavity of the either ring maintains relatively high electron density, in all cases (**Fig. 5)**, except for the tetranitro derivative where the electron withdrawing effect of the nitro groups cause relatively low electron density in the ether cavity.

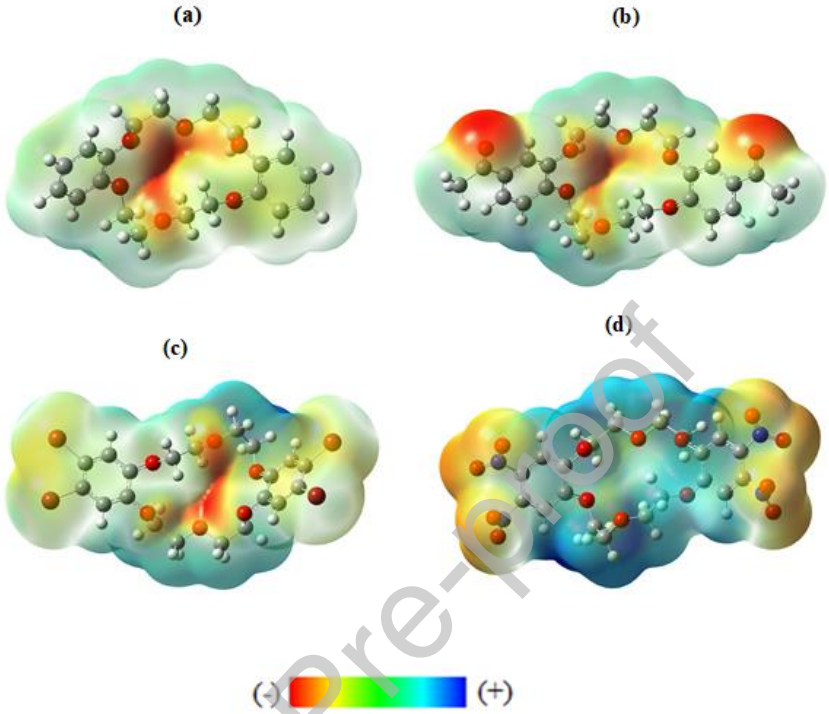

Fig. 5. Electrostatic potential maps for (a) DB18C6, (b) DB18C6diacetate, (c) tetrabromo DB18C6, (d) tetranitroDB18C6.

These results indicate that lead(II) ions are most likely to coordinate with the ether cavity of all systems except for the tetranitro derivative, where coordination is more probable at the nitro groups. The high electron density of the carbonyl oxygens, relative to the ether cavity of the diacetate compound (**Fig. 5(b)**), suggest possible exo-cavity coordination. However, the "well-like" shape of the ether cavity should facilitate the formation of a more stable complex with Pb^{2+} relative to that possible due to coordination at the C=O moieties. Hence, endo-cavity coordination is expected to be most probable. Similarly, high electron density on the bromine atoms, of the tetrabromo derivative, suggest that there could be exo-cavity metal binding or even a combination of exo- and endo- cavity binding. However, for a more comprehensive understanding of the Pb^{2+} binding behaviour of these systems, additional data is required.

Therefore, lead(II) nitrate was added in a step-wise manner to solutions of all compounds, whilst collecting the absorption spectra of the resulting solutions (uv-vis titration). Hence, a plot of absorbance versus metal: ligand ratio (mole ratio plot) was derived in all cases (**See S4**), revealing a 2:1 metal: ligand binding ratio for the tetrabromo derivative but a 1:1 ratio for the other compounds (**Table 1**).

Table 1. Lead(II) complexation thermodynamic parameters for DB18C6 derivatives at 298 K.

Compound	Ratio	Log K_{as}	ΔG^{o}_{as}/ (kJ mol^{-1})	ΔH_{as}/ R (K^{-1})	ΔS_{as}/R
DB18C6	1:1	3.56 ± 0.01	-20.32	18462.5 ± 610.8	70.1 ± 2.1
Tetrabromo-	2:1	5.17 ± 0.08	-29.49	25777.4 ± 2922.2	98.8 ± 9.8
Tetranitro-	1:1	2.79 ± 0.06	-16.02	3648.6 ± 313.5	18.6 ± 1.1
Diacetate-	1:1	3.84 ± 0.03	-21.89	21487.5 ± 3198.0	80.8 ± 10.7

From the mole ratio plots, Hill plots were derived for all compounds (**See S4**), allowing determination of their association constants (K_{as}) with Pb^{2+} and hence, the free energy change (ΔG^{o}_{as}) associated with such interactions (**Table 1**). Since all complexation potentials are exergonic; spontaneous binding of lead(II) ions with all derivatives is indicated. Expectedly however, the least negative value is calculated for the tetranitro derivative, indicating weak metal-ligand interactions relative to the other compounds. This is ascribed to complexation occurring *via* coordination at the nitro groups which are weakly basic; that is, poorly electron donating. Interestingly, whereas the lead(II) complexation potentials for DB18C6 and the diacetate derivative are comparable, formation of the Pb^{2+}-tetrabromo DB18C6 complex is most probable (**Table 1**). Optimization of Pb^{2+}-DB18C6 complex in acetonitrile, using the 6-311++G(d,p)/RB3LYP model chemistry, for all atoms except Pb^{2+}, where the LANL2DZ ECP was applied, allowed calculation of the complexation potential *via* $\Delta G^{o}_{as} = G_{com} - G_{g} - G_{h}$ where G_{com}, G_{g} and G_{h}, represent the absolute free energies of the complex, Pb^{2+} (guest) and the DB18C6 (host), respectively. The calculated association potential: -140 kJ mol^{-1}, though attractive (exergonic), is significantly less than that adduced experimentally (**Table**

1). Interestingly, this value is similar to that reported for the complexation of alkali metals: Li^+ to Cs^+, with DB18C6 [32]. However, despite exploration of several other model chemistries: 6-311G(d,p)/CAM-RB3LYP, 6-311++G(2d,p)/CAM-RB3LYP, 6-31++G(d,p)/CAM-RB3LYP, no improvement in this value was achieved. Such under estimation of the complexation potential is most likely due to the absence of direct solvent coordination effects, a factor well known to be highly influential in host-guest interactions [54]. Furthermore, since the guest is charged, stabilization from solvation effects are most likely significant.

The effect of temperature on the K_{as} values was also investigated via variable temperature uv-vis titrations and the resulting values applied *via* Van 't Hoff plots (**See S5**), in calculating the association enthalpy (ΔH_{as}) and entropy (ΔS_{as}) changes for all compounds. Unexpectedly, positive entropy values are observed for all systems (**Table 1**), suggesting that solvent rearrangement, as the separately hydrated host and guess species combine, plays a critical role in the complexation thermodynamics and hence, Pb^{2+} complexation probability of these ether systems. Hence, greater solvent rearrangement for the tetrabromo complexes where two metal ions are involved, leads to significant disorder in the solvent, hence, ΔS_{as} is most favourable (**Table 1**). That the formation of all complexes is endothermic, yet exergonic, the dominance of entropy in determining their Pb^{2+} absorption behaviour is highlighted. For the tetranitro derivative, coordination at the nitro groups probably requires minimal solvent rearrangement, hence, ΔS_{as} is least positive for this compound, thus, its formation is less probable.

3.3 Electrochemical behaviour

Cyclic and square wave voltammograms, collected for all compounds in acetonitrile (HPLC grade ≥ 99.9), show at least one anodic peak in the region of 1.4 to 2.2 V for both oxidatively (O) and reductively (R) initiated scans (**Fig. 6**). For instance, the cyclic voltammogram for DB18C6 shows a single oxidation at *ca*. 1.65 V with no corresponding reduction wave, even at very high or low scan rates (ν), indicating that this electron transfer (E) is followed by a very fast chemical process(C): EC mechanism, hence, this oxidation is irreversible. Furthermore, since a plot of current (I) versus $\nu^{1/2}$ is linear (R^2 = 0.98, **See S6**), it is reasonable to conclude that the processes associated with this oxidation are diffusion controlled, as suggested by the appropriate form of the popular Randles-Ševčík model [55,56]. Additionally, since the square wave voltammogram reveal a peak area which is

basically identical to that for ferrocene, under similar conditions, it can be reasonably concluded that the charge involved in this process is similar to that associated with the oxidation of ferrocene; a well-known one electron process [57].

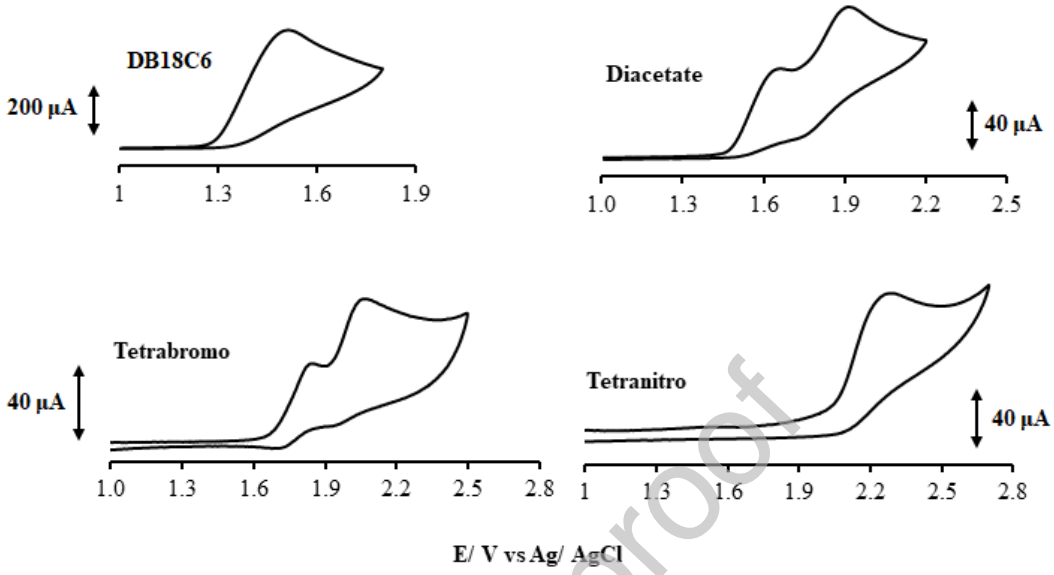

Fig. 6. Oxidatively initiated cyclic voltammograms for all compounds [Conc. 1 mM].

Calculated ground state MO surfaces (**Fig. 4**), for DB18C6, show that the HOMO is localized over the *pi*-system of a single phenyl ring, in addition to the oxygen atoms which are directly attached to that ring. Hence, reaction with a solvent molecule subsequent to the formation of a radical: EC mechanism, is most probable at the phenyl ring or at the directly attached ether oxygens. The presence of an acetate group on the phenyl rings result in an additional one electron diffusion controlled, irreversible oxidation at 1.91 V (**Fig. 6**), due to the loss of an *n*-electron from the acetate oxygen, as suggested by the calculated MO surfaces. Similarly, for the tetrabromo derivative, two oxidations are obvious: 2.03 and 1.87 V (**Fig. 6**), due to the loss of three electrons, most likely from the aromatic rings, since the *n*-electrons of the high electron density halogen atoms tend to conjugate with the aromatic *pi*-system, thereby increasing the electron density therein. In addition to a single diffusion controlled irreversible oxidation at 2.21 V, associated with electron loss from the aromatic *pi*-system of a single phenyl ring, the voltammogram for the tetranitro derivative is characterized by two successive quazi-reversible one electron reductions at: -0.87 and -1.49 V; for which the corresponding oxidations are observed at -0.98 and -0.74 V, respectively, due to the redox activity of the NO_2 group, as is typical for *o*-dinitrobenzene compounds [58]. These results

indicate that the redox behaviour of DB18C6 derivatives is highly dependent of the chemistry of the aromatic rings, effects which might affect their redox behaviour in the presence of lead(II) ions.

Hence, electropolymerization was attempted, for all compounds, *via* repeated CV scans (cycling). The repetitive voltammetric scans show significant changes on each cycle, for all compounds, except for the tetranitro derivative. For example, the oxidation, originally observed at 1.65 V for DB18C6, as discussed in the foregoing, shows significant reduction in current after the first cycle (**Fig. 7**); subsequent cycles resulting in a continuous and uniform current decay, concomitant with a shift to lower energy: 1.4 V.

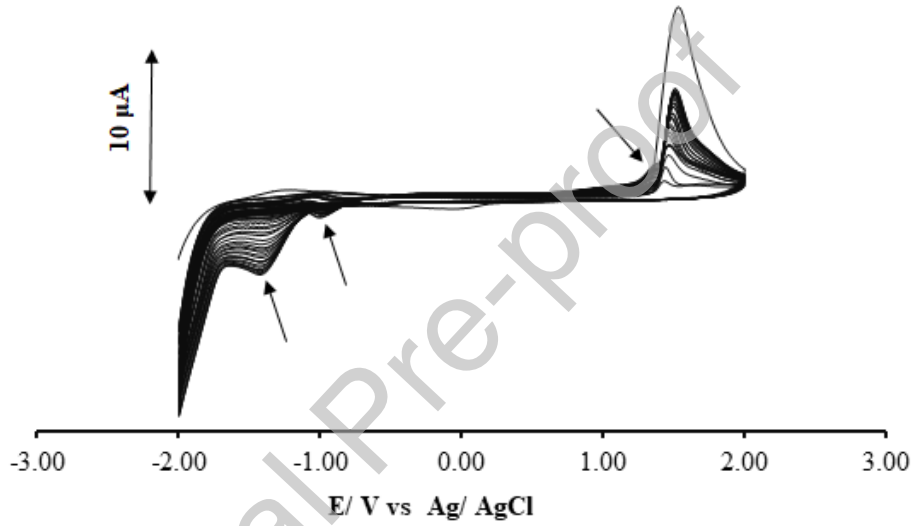

Fig. 7. Repeated cyclic voltammetry scans (30 scans at ν = 200 mV/ s) used to effect polymerization of DB18C6 [Conc. 1 mM in acetonitrile].

Interestingly, these changes are simultaneous with the emergence and progressive growth of two reductions at *ca*. -1.40 and *ca*. -0.99 V (**Fig. 7**); the emergence of which is indicative of the formation of a new electro active material, increasing in concentration to a point of saturation whilst the parent material: DB18C6 in this case, is depleted at the electrode surface due to its progressing electro-transformation. Such changes are consistent with electropolymerization [59]. For the other derivatives, similar changes, albeit more subtle, are obvious (**See S7**). The voltammogram for the tetrabromo derivative, for instance, shows two new reduction bands: -1.36 and -0.94 V, in addition to a new oxidation at 0.39 V, which shows saturation after ~6 to 10 cycles. Similarly, polymerization of the diacetate derivative on the electrode surface is suggested by significant reduction in the intensities of both

oxidation bands, originally observed at 1.65 and 1.91 V (*vide supra*) and their replacement by two new oxidations at 1.56 and 1.79 V (**See S7**). However, for tetranitro derivative, though there are slight changes in the position of the original peaks, no new peaks are observed (**See S7**), nonetheless, the slight current decay for the original peaks, on each cycle, is indicative of progressive electrode surface passivation. These observations indicate that instead of polymerization, the tetranitro derivative probably forms a stable chemisorbed coating on the electrode surface. Surely, such differences in the nature of the electrode surface passivation could significantly affect its response to the presence of Pb^{2+}, hence, electrode surface coverage (Γ) for each modified electrode is investigated based on

$$I_p = \frac{n^2 F^2 A\Gamma(\nu)}{4RT}$$

where, **Ip**, **n** and **F** represents the peak current, the number of electrons transferred on oxidation/ reduction of the analyte (Analyte = ferrocene where n = 1) and Faraday's constant, respectively. **A** is the electrode surface area whereas **R** and **T** represent the universal gas constant and the temperature. For all compounds, plots of **Ip** versus **ν** are linear, as expected (R2 ~ 0.99 – 0.97), and the calculated Γ values are in the range of 10^{-11} – 10^{-12} mol cm^{-2}, similar to values reported for monolayer coverage [60,61]. Since a Γ value of 1.22 x 10^{-11} mol cm^{-2} was determined experimentally for the tetranitro derivative whereas, that calculated based on the area of the optimized structure is 2.169 x 10^{-10} mol cm^{-2}, it is clear that the area of this compound, when adsorbed to the electrode surface, is larger than that estimated from molecular modelling (*vide supra*). This is most likely due to increase planarity of the structure on the electrode surface caused by strong interactions between the electrode surface and the nitro groups; a surface driven shift in the equilibrium molecular geometry. For the other compounds, experimentally determined Γ values are of the order 10^{-12}, also indicating significant differences in molecular orientation on the electrode surface. Indeed, this is expected since, the majority of evidence suggest that they undergo electro-polymerization, resulting in an immobilized polymeric coating on the electrode surface. Surely, such modification of the electrode surface should affect its ability to interact with lead(II) ions. Furthermore, the structural difference in these coating materials should be reflected in the behaviour of these electrodes, where the quantification of Pb^{2+} is concerned.

Therefore, differential pulse anodic stripping voltammetric (DPASV) studies, a very experienced and sensitive method, was carried out to assess the usefulness of these modified electrodes for the quantification of Pb^{2+} in aqueous solution. DPASV scans with a DB18C6-functionalized platinum working electrode show a well-defined peak at *ca*. -0.72 V in the presence of lead(II) ions (**Fig. 8(a)**), whose intensity (current) increases linearly with Pb^{2+} concentration (**Fig. 8(b)**), as opposed to the bare electrode where a very asymmetric band is observed at ca. 0.79 V, in addition to another broad band at ca. 0.46 V; none of which show a clear trend with Pb^{2+} concentration.

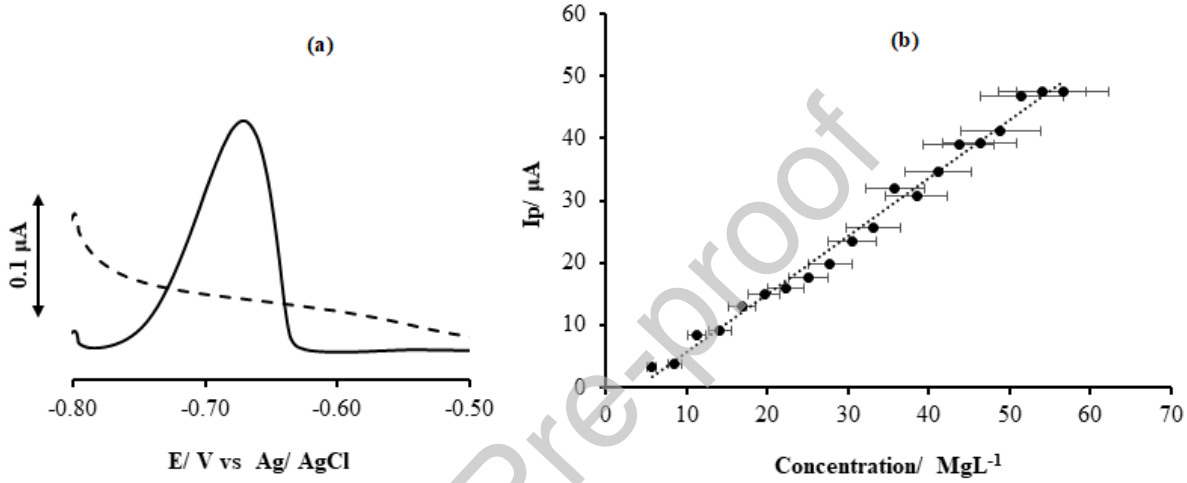

Fig. 8. (a) DPASV scan for a solution will $[Pb^{2+}] = 0$ (dashed line) and $[Pb^{2+}] = 1$ mM (solid line). (b) Calibration curve derived from the DPASV results for DB18C6. The pH was maintained by an acetate-acetic acid buffer system.

Therefore, current response as function of $[Pb^{2+}]$ was measured using all modified electrodes (**See S8**) at a pH value: 4.5, where current response is maximum. The linear regression method was then applied in determining the limits of detection (LOD) and quantification (LOQ) as well as the linear ranges (LR) for all modified electrodes (**Table 2**). Interestingly, the DB18C6 electrode offers the lowest LOQ and LOD, followed by the tetrabromo derivative which also offers a slightly wider linear range than the other electrodes. The wider linear range observed for the tetrabromo DB18C6 electrode might be a result of its ability to interact with Pb^{2+} in 2:1 metal: ligand ratio. Expectedly, the electron withdrawing nature of the nitro groups which prevent interactions between lead ions and the ether cavity, in addition to the weak metal-nitro group interactions, not only result in one of the narrowest linear ranges but also the highest LOD and LOQ (**Table 2**), clear indications of its inferior sensitivity.

Table 2. Linear range, limits of detection and quantification adduced from the calibration curves of current versus [Pb^{2+}] for the different functionalized electrodes.

Compound	LR/ mg L^{-1}	LOD/ mg L^{-1}	LOQ/ mg L^{-1}
DB18C6	8.49 – 56.60	3.06	9.27
Diacetate	5.68 – 59.14	5.27	15.97
Tetrabromo	2.85 – 59.14	4.56	13.38
Tetranitro	2.85 – 54.05	11.11	33.65

These results clearly show that the compounds investigated in this study holds real potential for application in the preparation of modified electrodes for the electrochemical detection and quantification of lead(II) ions in aqueous solution. However, "real-life" samples are often contaminated with other electrolytes which can significantly impact the results adduced from such electrodes. Therefore, DPASV scans in the presence of a mixture of various other metals ions were collected at ambient temperature, for all electrodes: interference study. The presence of other metal ions resulted in slight potential shifts of the lead peak, however, since current is the parameter applied in the quantification of Pb^{2+}, such slight changes in peak potential are inconsequential. Changes in the current on addition of each metal ion to the mixture are obvious (**Fig.** 9), however, all changes are such that the current values are of the same order of magnitude as that for Pb^{2+} in pure water, hence, the Pb^{2+} concentration adduced, in most cases, will not be significantly affected. Though the presence of other metal ions leads to current fluctuation between 3.18×10^{-5} and 2.59×10^{-5}: minor changes, the presence on mercury(II) ions leads to significant changes (increase) in the current for DB18C6, DB18C6diacetate and the tetranitroDB18C6 electrodes (**Fig. 9(a)**). This indicates that these systems would suffer from a mercury error. Such effects might be due to significant coordination competition between Hg^{2+} and Pb^{2+}, resulting from entropic effects associated with solvent rearrangement energetics in the complexation process, in addition to the higher charge density of Hg^{2+} which allows stronger interactions with the hard donor sites of these ether systems.

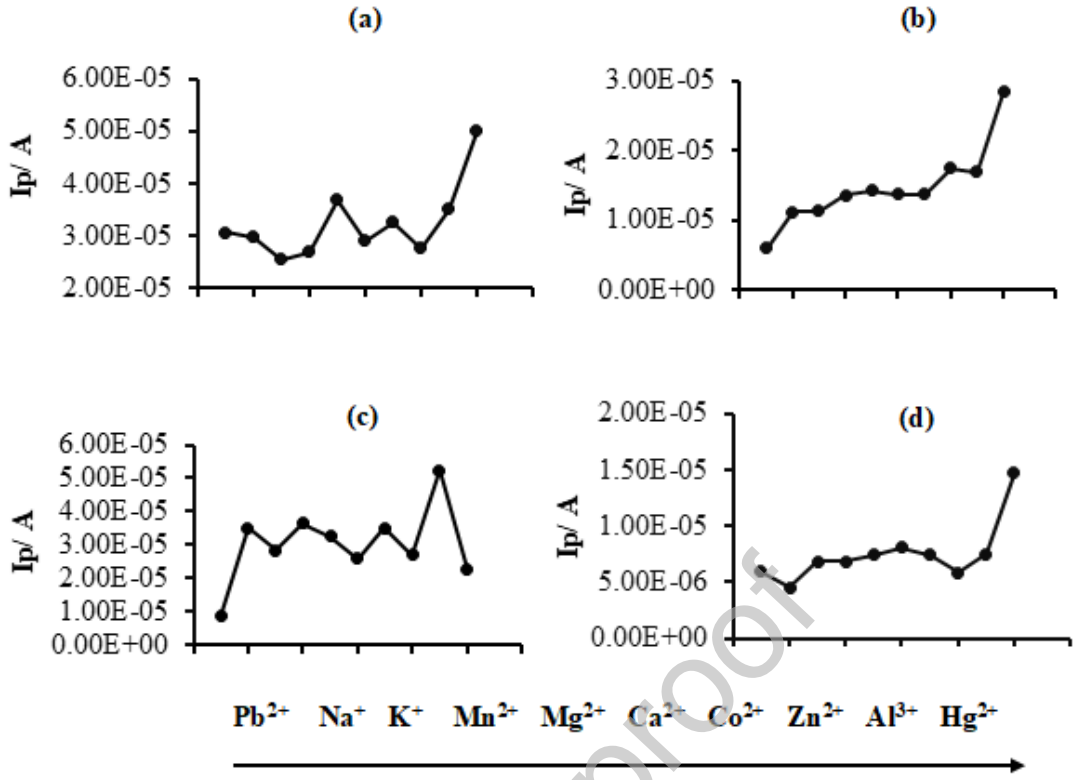

Fig. 9. Effects of presence of other metal ions [Conc. 10 ppm] on the current response obtained for lead [Conc. 50 ppm] when the electrode surface is modified with (a) DB18C6, (b) DB18C6diacetate, (c) TetrabromoDB18C6 and (d) TetranitroDB18C6. Solutions where buffered by sodium acetate-acetic acid mixture to maintain a pH of 4.5.

Interestingly, for electrodes prepared from the tetrabromo derivative, addition of Hg^{2+} ions does not cause a significant change in the current, however, the presence of Al^{3+} result in a noteworthy current spike (**Fig. 9 (c)**, albeit without a change in the order of magnitude of the signal. This is indicative of significant coordination competition between Pb^{2+} and Al^{3+}, most likely due to the significantly higher charge density of Al^{3+}, coupled with the entropic effects associated with solvent rearrangement during complexation.

4 Conclusion

Dibenzo-18-crown-6 and its diacetate, tetrabromo and tetranitro derivatives are able to spontaneously coordinate with lead(II) ions in their free monomeric form; a process controlled by entropic effects. Their ability to passivate a platinum electrode surface, *via* electropolymerization or chemisorption in the case of the tetranitro derivative, allows the preparation of modified electrodes, capable of quantifying lead(II) ion at concentrations below 10 mg L^{-1} with minimal errors in the presence of other metal ions, except for Al^{3+} and

Hg^{2+} which offers significant coordination competition to lead ions. Hence, where Al^{3+} and Hg^{2+} concentrations are significant, the results adduced from these modified electrodes will require correction. Nonetheless, they represent real prospects for fast and relatively cheap designing of plasticizer free Pb^{2+} ion selective electrodes for operation in aqueous media.

Acknowledgement

National Commission on Science and Technology, Jamaica for research funds provided to this research group.

Credit author statement

I hereby declare that the work presented in this manuscript was conducted solely by the three authors presented in the list of authors on the cover of the paper. The lead researcher Ms Deneikah Jackson who is a graduate student was responsible for collecting and analysing experimental data. She was also instrumental in preparing the manuscript. This work was carried out under the supervision of Peter Nattaniel Nelson who is the corresponding author. He was responsible for designing the project, analysing data, guiding the experimental process and preparing the manuscript for publication. The third author, Irvin Booysen was instrumental in analysing data, guiding the experimental process and helping to prepare the final manuscript.

The authors can, in all honesty, state that the work presented therein is original and does not copy from any other articles, written by any other authors, in full or part.

Declaration of interest statement

We, the authors of this manuscript, declare with absolute certainty that there is no conflict of interest concerning the work in this manuscript. The work presented therein is solely for academic purposes and was conducted by the authors listed on this manuscript.

Reference

[1] Gäbler, H. E.; Schneider, J., Assessment of heavy-metal contamination of floodplain soils due to mining and mineral processing in the Harz Mountains, Germany. *Environmental Geology* **2000,** *39* (7), 774-782.

[2] Dhakate, R.; Singh, V. S.; Hodlur, G. K., Impact assessment of chromite mining on groundwater through simulation modeling study in Sukinda chromite mining area, Orissa, India. *Journal of Hazardous Materials* **2008,** *160* (2), 535-547.

[3] Garcia-Sanchez, A.; Alvarez-Ayuso, E., Arsenic in soils and waters and its relation to geology and mining activities (Salamanca Province, Spain). *Journal of Geochemical Exploration* **2003,** *80* (1), 69-79.

[4] Coynel, A.; Schäfer, J.; Dabrin, A.; Girardot, N.; Blanc, G., Groundwater contributions to metal transport in a small river affected by mining and smelting waste. *Water Research* **2007,** *41* (15), 3420-3428.
[5] Théraulaz, F.; Thomas, O. P., Complexometric determination of mercury(II) in waters by spectrophotometry of its dithizone complex. *Microchimica Acta* **1994,** *113* (1), 53-59.
[6] Tsunogai, S.; Nishimura, M.; Nakaya, S., Complexometric titration of calcium in the presence of larger amounts of magnesium. *Talanta* **1968,** *15* (4), 385-390.
[7] Zhai, J.; Xie, X.; Bakker, E., Ionophore-based ion-exchange emulsions as novel class of complexometric titration reagents. *Chemical Communications* **2014,** *50* (84), 12659-12661.
[8] Lyle, S. J.; Rahman, M. M., Complexometric titration of yttrium and the lanthanons—I: A comparison of direct methods. *Talanta* **1963,** *10* (11), 1177-1182.
[9] Leray, I.; Valeur, B., Calixarene-Based Fluorescent Molecular Sensors for Toxic Metals. *European Journal of Inorganic Chemistry* **2009,** *2009* (24), 3525-3535.
[10] Adhikari, B. B.; To, C.-A.; Iwasawa, T.; Schramm, M. P., Pb, Sr and Ba calix[6]arene hexacarboxylic acid octahedral complexation: a dramatic effect of dealkylation. *Supramol Chem* **2015,** *27* (10), 724-730.
[11] Talanova, G. G.; Elkarim, N. S. A.; Talanov, V. S.; Bartsch, R. A., A Calixarene-Based Fluorogenic Reagent for Selective Mercury(II) Recognition. *Analytical Chemistry* **1999,** *71* (15), 3106-3109.
[12] Métivier, R.; Leray, I.; Valeur, B., Lead and Mercury Sensing by Calixarene-Based Fluoroionophores Bearing Two or Four Dansyl Fluorophores. *Chemistry – A European Journal* **2004,** *10* (18), 4480-4490.
[13] Ghosh, P.; Bharadwaj, P. K.; Roy, J.; Ghosh, S., Transition Metal (II)/(III), Eu(III), and Tb(III) Ions Induced Molecular Photonic OR Gates Using Trianthryl Cryptands of Varying Cavity Dimension. *Journal of the American Chemical Society* **1997,** *119* (49), 11903-11909.
[14] Muthukumar, C.; Kesarkar, S. D.; Srivastava, D. N., Conductometric mercury [II] sensor based on polyaniline–cryptand-222 hybrid. *Journal of Electroanalytical Chemistry* **2007,** *602* (2), 172-180.
[15] Pouretedal, H. R.; Shamsipur, M., A PVC-based cryptand C2B22 membrane potentiometric sensor for zinc(II). *Fresenius' Journal of Analytical Chemistry* **1998,** *362* (4), 415-418.
[16] Sadhu, K. K.; Sen, S.; Bharadwaj, P. K., Cryptand derived fluorescence signaling systems for sensing Hg(ii) ion: A comparative study. *Dalton Transactions* **2011,** *40* (3), 726-734.
[17] Gokel, G. W.; Leevy, W. M.; Weber, M. E., Crown Ethers: Sensors for Ions and Molecular Scaffolds for Materials and Biological Models. *Chemical Reviews* **2004,** *104* (5), 2723-2750.
[18] Suzuki, Y.; Morozumi, T.; Nakamura, H.; Shimomura, M.; Hayashita, T.; Bartsh, R. A., New Fluorimetric Alkali and Alkaline Earth Metal Cation Sensors Based on Noncyclic Crown Ethers by Means of Intramolecular Excimer Formation of Pyrene. *The Journal of Physical Chemistry B* **1998,** *102* (40), 7910-7917.
[19] Maeda, H.; Tierney, D. L.; Mariano, P. S.; Banerjee, M.; Cho, D. W.; Yoon, U. C., Lariat-crown ether based fluorescence sensors for heavy metal ions. *Tetrahedron* **2008,** *64* (22), 5268-5278.
[20] Hayashita, T.; Teramae, N.; Kuboyama, T.; Nakamura, S.; Yamamoto, H.; Nakamura, H., Chromoionophores Based on Crown Ethers and Related Structures for Alkali Metal Ion Sensing in Aqueous Media. *Journal of inclusion phenomena and molecular recognition in chemistry* **1998,** *32* (2), 251-265.

[21] Xie, J.; Ménand, M.; Maisonneuve, S.; Métivier, R., Synthesis of Bispyrenyl Sugar-Aza-Crown Ethers as New Fluorescent Molecular Sensors for Cu(II). *The Journal of Organic Chemistry* **2007,** *72* (16), 5980-5985.
[22] Huang, M.; Ma, X.; Li, X., Macrocyclic compound as ionophores in lead(II) ion-selective electrodes with excellent response characteristics. *Chinese Science Bulletin* **2008,** *53* (21), 3255.
[23] Shamsipur, M.; Ganjali, M. R.; Rouhollahi, A., Lead-selective membrane potentiometric sensor based on an 18-membered thiacrown derivative. *Anal Sci* **2001,** *17* (8), 935-938.
[24] Bocheńska, M.; Guziński, M.; Kulesza, J., Lower Rim Substituted p-tert-Butyl-Calix[4]arene. Part 15. Pb(II)-Ion-Selective Electrodes Based on p-tert-Butyl-calix[4]arene Thioamides. *Electroanalysis* **2009,** *21* (17-18), 2054-2060.
[25] (a) Kulesza, J.; Alves Júnior, S.; Guziński, M.; Bocheńska, M.; Hubscher-Bruder, V.; Arnaud-Neu, F., Calix[4]Arenes Appended with Thioamide Moieties as Powerful Tool for Heavy Metals Recognition. *Advances in Science and Technology* **2013,** *77*, 77-81; (b) Dai, Y.; Liu, C. C., A Simple, Cost-Effective Sensor for Detecting Lead Ions in Water Using Under-Potential Deposited Bismuth Sub-Layer with Differential Pulse Voltammetry (DPV). *Sensors (Basel)* **2017,** *17* (5), 950.
[26] Jackson, D. T.; Nelson, P. N., Preparation and properties of some ion selective membranes: A review. *Journal of Molecular Structure* **2019,** *1182*, 241-259.
[27] Boda, A.; Ali, S. M.; Shenoi, M. R. K.; Rao, H.; Ghosh, S. K., DFT modeling on the suitable crown ether architecture for complexation with Cs+ and Sr2+ metal ions. *Journal of Molecular Modeling* **2011,** *17* (5), 1091-1108.
[28] More, M. B.; Ray, D.; Armentrout, P. B., Intrinsic Affinities of Alkali Cations for 15-Crown-5 and 18-Crown-6: Bond Dissociation Energies of Gas-Phase M+−Crown Ether Complexes. *Journal of the American Chemical Society* **1999,** *121* (2), 417-423.
[29] Chu, I.-H.; Zhang, H.; Dearden, D. V., Macrocyclic chemistry in the gas phase: intrinsic cation affinities and complexation rates for alkali metal cation complexes of crown ethers and glymes. *Journal of the American Chemical Society* **1993,** *115* (13), 5736-5744.
[30] Anderson, J. D.; Paulsen, E. S.; Dearden, D. V., Alkali metal binding energies of dibenzo-18-crown-6: experimental and computational results. *International Journal of Mass Spectrometry* **2003,** *227* (1), 63-76.
[31] Maleknia, S.; Brodbelt, J., Gas-phase selectivities of crown ethers for alkali metal ion complexation. *Journal of the American Chemical Society* **1992,** *114* (11), 4295-4298.
[32] Choi, C. M.; Heo, J.; Kim, N. J., Binding selectivity of dibenzo-18-crown-6 for alkali metal cations in aqueous solution: A density functional theory study using a continuum solvation model. *Chem Cent J* **2012,** *6* (1), 84-84.
[33] (a) Jones, R. L.; Homa, D. M.; Meyer, P. A.; Brody, D. J.; Caldwell, K. L.; Pirkle, J. L.; Brown, M. J., Trends in Blood Lead Levels and Blood Lead Testing Among US Children Aged 1 to 5 Years, 1988–2004. *Pediatrics* **2009,** *123* (3), e376; (b) Pieper, K. J.; Tang, M.; Edwards, M. A., Flint Water Crisis Caused By Interrupted Corrosion Control: Investigating "Ground Zero" Home. *Environmental Science & Technology* **2017,** *51* (4), 2007-2014.
[34] Pieper, K. J.; Martin, R.; Tang, M.; Walters, L.; Parks, J.; Roy, S.; Devine, C.; Edwards, M. A., Evaluating Water Lead Levels During the Flint Water Crisis. *Environmental Science & Technology* **2018,** *52* (15), 8124-8132.
[35] Barn, P.; Kosatsky, T., Lead in School Drinking Water: Canada Can and Should Address This Important Ongoing Exposure Source. *Canadian Journal of Public Health* **2011,** *102* (2), 118-121.
[36] Patel, H. A., Proton Conduction in Tröger's Base-Linked Poly(crown ether)s. **2018,** *10* (30), 25303-25310.

[37] Rey Eliseo, C. T.; Grace, M. N.; Arnel, B. B.; Myoung Jun, P.; Basavaraj, R. P.; Seong-Poong, L.; Jeong Gil, S.; Wook-Jin, C., Microwave-Assisted Synthesis of Dibenzo-Crown Ethers. *Letters in Organic Chemistry* **2014,** *11* (2), 109-115.
[38] M. J. Frisch, G. W. T., H. B. Schlegel, G. E. Scuseria, M. A. Robb, J. R. Cheeseman, G. Scalmani, V. Barone, G. A. Petersson, H. Nakatsuji, X. Li, M. Caricato, A. V. Marenich, J. Bloino, B. G. Janesko, R. Gomperts, B. Mennucci, H. P. Hratchian, J. V. Ortiz, A. F. Izmaylov, J. L. Sonnenberg, D. Williams-Young, F. Ding, F. Lipparini, F. Egidi, J. Goings, B. Peng, A. Petrone, T. Henderson, D. Ranasinghe, V. G. Zakrzewski, J. Gao, N. Rega, G. Zheng, W. Liang, M. Hada, M. Ehara, K. Toyota, R. Fukuda, J. Hasegawa, M. Ishida, T. Nakajima, Y. Honda, O. Kitao, H. Nakai, T. Vreven, K. Throssell, J. A. Montgomery, Jr., J. E. Peralta, F. Ogliaro, M. J. Bearpark, J. J. Heyd, E. N. Brothers, K. N. Kudin, V. N. Staroverov, T. A. Keith, R. Kobayashi, J. Normand, K. Raghavachari, A. P. Rendell, J. C. Burant, S. S. Iyengar, J. Tomasi, M. Cossi, J. M. Millam, M. Klene, C. Adamo, R. Cammi, J. W. Ochterski, R. L. Martin, K. Morokuma, O. Farkas, J. B. Foresman, and D. J. Fox, Gaussian 16, Revision B.01. **2016**.
[39] Becke, A. D., Density-functional thermochemistry. III. The role of exact exchange. *Journal of Chemical Physics* **1993,** *98*, 5648.
[40] Lee, C.; Yang, W.; Parr, R. G., Development of the Colle-Salvetti correlation-energy formula into a functional of the electron density. *Physical Review B* **1988,** *37* (2), 785-789.
[41] Yanai, T.; Tew, D. P.; Handy, N. C., A new hybrid exchange–correlation functional using the Coulomb-attenuating method (CAM-B3LYP). *Chemical Physics Letters* **2004,** *393* (1), 51-57.
[42] Cossi, M.; Rega, N.; Scalmani, G.; Barone, V., Polarizable dielectric model of solvation with inclusion of charge penetration effects. *The Journal of Chemical Physics* **2001,** *114* (13), 5691-5701.
[43] Cossi, M.; Rega, N.; Scalmani, G.; Barone, V., Energies, structures, and electronic properties of molecules in solution with the C-PCM solvation model. *Journal of computational chemistry* **2003,** *24* (6), 669-81.
[44] Hay, P. J.; Wadt, W. R., Ab initio effective core potentials for molecular calculations. Potentials for the transition metal atoms Sc to Hg. *The Journal of Chemical Physics* **1985,** *82* (1), 270-283.
[45] Wadt, W. R.; Hay, P. J., Ab initio effective core potentials for molecular calculations. Potentials for main group elements Na to Bi. *The Journal of Chemical Physics* **1985,** *82* (1), 284-298.
[46] Nelson, P. N.; Ellis, H. A., Structural, odd–even chain alternation and thermal investigation of a homologous series of anhydrous silver(i) n-alkanoates. *Dalton Transactions* **2012,** *41* (9), 2632-2638.
[47] Nelson, P. N.; Taylor, R. A., Theories and experimental investigations of the structural and thermotropic mesomorphic phase behaviors of metal carboxylates. *Applied Petrochemical Research* **2014,** *4* (3), 253-285.
[48] Nelson, P. N.; Ellis, H. A.; Taylor, R. A., Effects of molecular and lattice structure on the thermal behaviours of some long chain length potassium(I) n-alkanoates. *Journal of Molecular Structure* **2014,** *1058*, 234-243.
[49] Bernstein, H. J., Bond distances in hydrocarbons. *Transactions of the Faraday Society* **1961,** *57* (0), 1649-1656.
[50] A. C. Alves, J.; V. Barkley, J.; F. Brigas, A.; A. W. Johnstone, R., Metal-assisted reactions. Part 26.1 Catalytic reactivity and ether bond lengths in aryloxytetrazoles and aryloxypseudosaccharins. *Journal of the Chemical Society, Perkin Transactions 2* **1997,** (4), 669-678.

[51] Trotter, J., Bond lengths in benzene derivatives: Hybridization or resonance. *Tetrahedron* **1960,** *8* (1), 13-22.
[52] Kusaka, R.; Inokuchi, Y.; Ebata, T., Structure of hydrated clusters of dibenzo-18-crown-6-ether in a supersonic jet—encapsulation of water molecules in the crown cavity. *Physical Chemistry Chemical Physics* **2008,** *10* (41), 6238-6244.
[53] Robert M. Silverstein, F. X. W., David J. Kiemle, David L. Bryce, *Spectrometric Identification of Organic Compounds*. 8 ed.; Wiley: 2014; p 464.
[54] Glendening, E. D.; Feller, D.; Thompson, M. A., An Ab Initio Investigation of the Structure and Alkali Metal Cation Selectivity of 18-Crown-6. *Journal of the American Chemical Society* **1994,** *116* (23), 10657-10669.
[55] Randles, J. E. B., A cathode ray polarograph. Part II.—The current-voltage curves. *Transactions of the Faraday Society* **1948,** *44* (0), 327-338.
[56] Ševčík, A., Oscillographic polarography with periodical triangular voltage. *Collect. Czech. Chem. Commun.* **1948,** *13*, 349-377.
[57] Zanello, P.; Cinquantini, A.; Mangani, S.; Opromolla, G.; Pardi, L.; Janiak, C.; Rausch, M. D., The redox behaviour of ferrocene derivatives: VI. Benzylferrocenes. The crystal structure of decabenzylferrocenium tetrafluoroborate. *Journal of Organometallic Chemistry* **1994,** *471* (1), 171-177.
[58] Chambers, J. Q.; Adams, R. N., Nitro-group elimination in the reduction of dinitrobenzenes in dimethylformamide. *Journal of Electroanalytical Chemistry (1959)* **1965,** *9* (5), 400-407.
[59] Tanaka, K.; Shichiri, T.; Wang, S.; Yamabe, T., A study of the electropolymerization of thiophene. *Synthetic Metals* **1988,** *24* (3), 203-215.
[60] Bard, A. J., Chemical modification of electrodes. *Journal of Chemical Education* **1983,** *60* (4), 302.
[61] Untereker, D. F.; Lennox, J. C.; Wier, L. M.; Moses, P. R.; Murray, R. W., Chemically modified electrodes: Part IV. Evidence for formation of monolayers of bonded organosilane reagents. *Journal of Electroanalytical Chemistry and Interfacial Electrochemistry* **1977,** *81* (2), 309-318.

Graphical Abstract